IEEE Photonics Journal
An IEEE Photonics Society Publication

Distinct Lasing Operation From Chirped InAs/InP Quantum-Dash Laser

Volume 5, Number 4, August 2013

M. Z. M. Khan
T. K. Ng, Member, IEEE
Chi-Sen Lee
D. H. Anjum
D. Cha
P. Bhattacharya, Fellow, IEEE
B. S. Ooi, Senior Member, IEEE

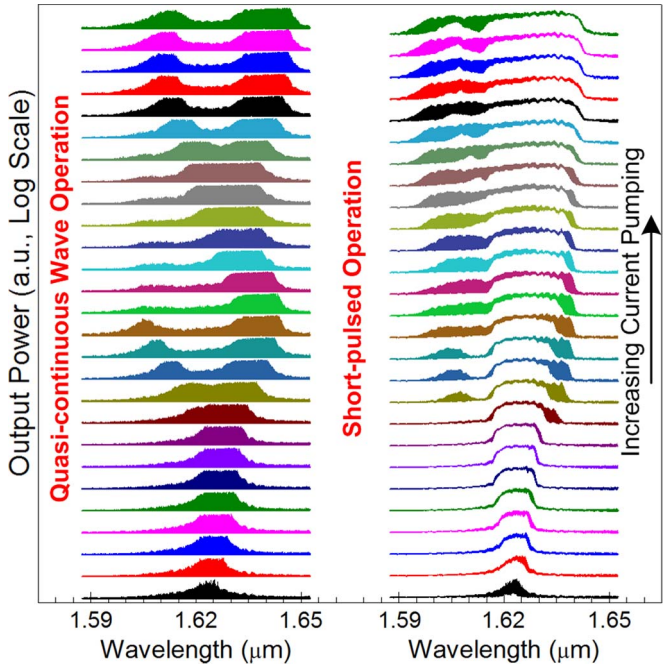

DOI: 10.1109/JPHOT.2013.2272781
1943-0655/$31.00 ©2013 IEEE

Distinct Lasing Operation From Chirped InAs/InP Quantum-Dash Laser

M. Z. M. Khan,[1] T. K. Ng,[1] *Member, IEEE*, Chi-Sen Lee,[2] D. H. Anjum,[3] D. Cha,[3] P. Bhattacharya,[2] *Fellow, IEEE*, and B. S. Ooi,[1] *Senior Member, IEEE*

[1]Photonics Laboratory, Computer, Electrical and Mathematical Science and Engineering Division, King Abdullah University of Science and Technology (KAUST), Thuwal 23955-6900, Saudi Arabia
[2]Department of Electrical Engineering and Computer Science, University of Michigan, Ann Arbor, MI 48109-2122 USA
[3]Advanced Nanofabrication and Imaging Core Laboratory, King Abdullah University of Science and Technology (KAUST), Thuwal 23955-6900, Saudi Arabia

DOI: 10.1109/JPHOT.2013.2272781

Manuscript received June 2, 2013; revised July 2, 2013; accepted July 3, 2013. Date of publication July 11, 2013; date of current version August 2, 2013. This work was supported by King Abdullah University of Science and Technology under Competitive Research Grant CRG-1-2012-OOI-010. Corresponding author: Boon S. Ooi (e-mail: boon.ooi@kaust.edu.sa).

Abstract: We study the enhanced inhomogeneity across the InAs quantum-dash (Qdash) layers by incorporating a chirped AlGaInAs barrier thickness in the InAs/InP laser structure. The lasing operation is investigated via Fabry–Pérot ridge-waveguide laser characterization, which shows a peculiar behavior under quasi-continuous-wave (QCW) operation. Continuous energy transfer between different dash ensembles initiated quenching of lasing action among certain dash groups, causing a reduced intensity gap in the lasing spectra. We discuss these characteristics in terms of the quasi-zero-dimensional density of states (DOS) of dashes and the active region inhomogeneity.

Index Terms: Semiconductor lasers, semiconductor quantum dots, quantum dash lasers, self-assembled quantum dot, inhomogeneous broadening.

1. Introduction

Recent demonstrations of self-assembled Qdash /quantum dot (Qdot) nanostructures as potential broad gain material system, via laser diodes [1]–[6], semiconductor optical amplifiers (SOA) [7], [8] and superluminescent diodes (SLD) [9], [10], have lead to the achievement of high performance devices for broad wavelength tunability applications. In particular, Qdash nanostructures based on InP substrate and related technology received considerable attention because of their wavelength span of ground state emission in the S–C–L international telecommunication unit bands [7], [11]. Moreover, the inherent dot- and wire-like characteristics of dashes, with large inhomogeneous broadening (IHB) resulted in the realization of broad gain bandwidth of ~300 nm from these nanostructures [12]. In device demonstration, broad amplified spontaneous emission (ASE) of ~140 nm have been reported from Qdash SOA and SLD [9], [10] utilizing fixed or varying Qdash monolayer thickness in a multi-stack epitaxial structure. Unlike the ASE related studies, extending lasing bandwidth through intentional IHB was also demonstrated with InAs/InGaAs Qdot laser, resulting in a broad emission spectrum of ~75 nm [5], [6], and recently, by our group, utilizing Qdash lasers [1]–[3]. A high power (~1 W per device), broadband (~41 nm) Qdash lasers in the C–L communication band highlighted the simultaneous achievement of high power and broad lasing bandwidth.

In this work, we further extend our exploration of different InAs/InP Qdash epitaxial structure in achieving high power and broadband stimulated emission devices. Instead of using a fixed

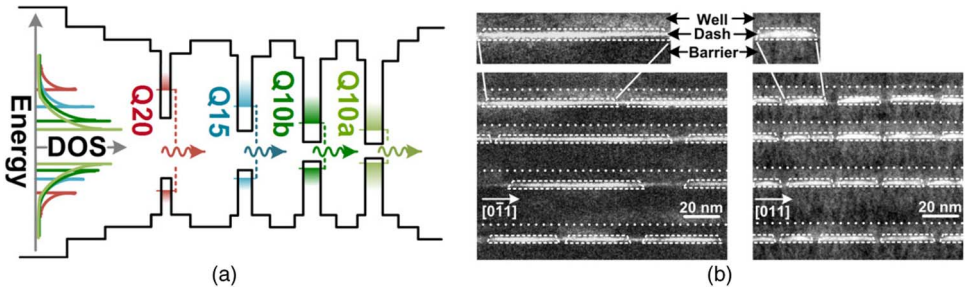

Fig. 1. (a) Energy band model revealing four Qdash groups corresponding to the four stacking layers, and (b) [0-11] and [011] cross-sectional TEM micrographs, of the chirped Qdash laser structure.

AlGaInAs barrier [1]–[3] in the multi-stack Qdash structure, here we utilized a varying barrier thickness (chirp) design, and investigated the spectral characteristics via ridge-waveguide laser under two pulsed modes. Contrary to the short pulse width (SPW) operation wherein a broadband and reasonably single lasing spectral lobe is observed, the QCW operation shows an anomalous lasing behavior (dual lasing lobe) at high injection, dictating presence of photon re-absorption process, and lasing action from different dash ensembles being influenced by junction temperature variation. Our analysis provides more insight to the Qdash device physics and help in realizing a viable ultra-wide lasing bandwidth and high power devices with optimized epitaxial design features. Highlighting the importance of such devices, they can find important applications in optical sensors, communications, spectroscopy, and highly sensitive optical gyroscope for medical, optical telecommunications, and military applications. Furthermore, high output power produced by these broadband lasers will enable broader applications in ultra-short pulse generation, and higher resolution biomedical imaging using optical coherence tomography technology [2], [7], [10], [13].

2. Material Characterization

The laser structure has 4 stacks of 5 monolayers InAs dashes, each embedded in a 7.6 nm compressively strained $In_{0.64}Ga_{0.16}Al_{0.20}As$ asymmetric quantum well, and a varying thickness (20, 15, 10, and 10 nm) tensile-strained $In_{0.50}Ga_{0.32}Al_{0.18}As$ top barriers, starting from a fixed 25 nm lower barrier. The details of the full structure can be found elsewhere [3], [4]. A simple energy band diagram of the chirped Qdash structure (CQD) is shown in Fig. 1(a) for better illustration. Another fixed barrier (10 nm) thickness multi-stack (FQD), and a single-stack (SQD), Qdash partial structures were also prepared for comparison purpose. Fig. 1(b) corresponds to the [011] and [0-11] cross-sectional transmission electron microscope (TEM) micrographs of the CQD sample with statistical average dash (bright truncated pyramids) height of the stacks $\sim$3 nm (top), $\sim$2.8 nm, $\sim$2.7 nm, and $\sim$2.5 nm (bottom), with an error margin of $\pm$ 0.5 nm. This qualitative analysis suggests that average dash size dispersion across the stacks fairly contribute to the enhanced IHB, apart from the compositional variation. We further investigate the effect of chirping the active region by photoluminescence (PL) spectroscopy.

The measurements were performed at 77 K using a 1064 nm diode pumped solid-state laser as excitation source. Referring to Fig. 2(a) and (b), at low excitation density, the ground state emissions at $\sim$1540 nm are identical in both CQD and FQD samples. The PL peak wavelength gradually blue shifted, and at 3000 W/cm^2 the emission wavelength from both structures are again seen to converge ($\sim$1462 nm) implying the dominant emission from the 10 nm barriers Qdash layer, *Q*10 with the long (short) emission wavelength attributed to the top *Q*10*a* (bottom *Q*10*b*) stacks. The strong modulation at $\sim$1430 nm might be attributed to the onset of second emission hump in CQD sample, probably an indication of emission from 15 nm barrier Qdash layer, *Q*15, since this characteristics is absent in FQD sample, as illustrated in Fig. 2(b). No appreciable emission from the thickest barrier dash layer (20 nm, *Q*20) is seen in Fig. 2(a) due probably to non-uniform carrier localization among inhomogeneously broadened dash ensembles, with less carriers filling the small

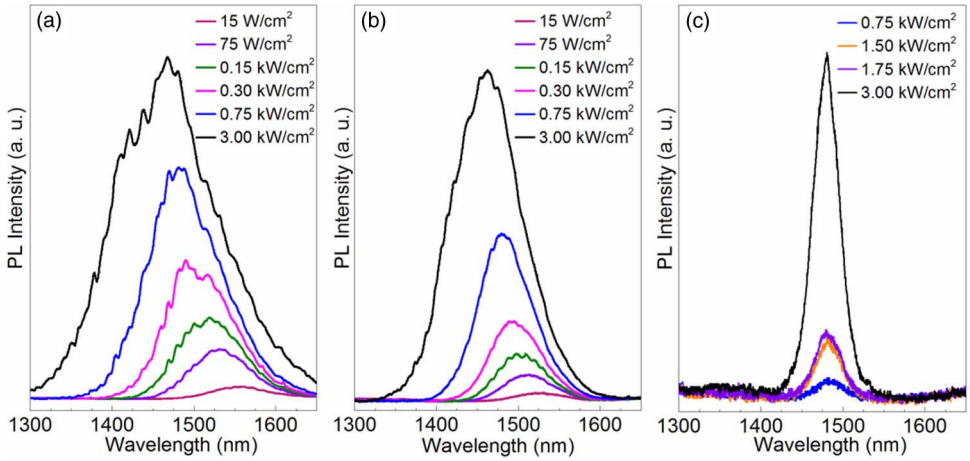

Fig. 2. Photoluminescence spectra measured at 77 K under increasing excitation power density for (a) CQD, (b) FQD, and (c) SQD samples.

average dash height *Q*20 layer compared to large average dash height layers [12], [14]. The PL spectra of both the multi-stack structures gradually broadens with increasing excitation, and for 3000 W/cm^2, the PL full width at half maximum (FWHM) of the CQD (146 nm) exceeds FQD (104 nm) by 42 nm. This significantly larger broadening of the PL spectra from CQD compared to FQD is a collective contribution from different multiple transition states appearing from the extended IHB among the dash layers. However, the excitation power density dependent PL of SQD sample, illustrated in Fig. 2(c), not only shows a negligible blue shift in the peak emission wavelength but also an insignificant increase in the FWHM. The peak wavelength and FWHM at 3000 W/cm^2 attains a value of $\sim$1480 nm and $\sim$39 nm, respectively, showing that the localized or in-plane inhomogeneity of an individual stack contributes a smaller broadening of the PL spectra compared to the inhomogeneity across the multi-stacks. Therefore, in our subsequent sections, we focus our discussion on the inhomogeneity across the stacking layers for ease in understanding.

3. Device Characterization

Ridge-waveguide laser diodes with ridge-width 2 μm and lengths 450-3000 μm with as-cleaved facets were fabricated and characterized at room temperature. Fig. 3(a) shows the $L-I$ characteristics of a 2×830 μm^2 CQD laser diode at 100 μs (QCW) and 0.5 μs (SPW) pulsed mode with 0.2% duty cycle. The corresponding modes progressive series of lasing spectra are shown in Fig. 3(b) and (c). The QCW (SPW) operation yield a threshold current density $J_{th} = 3.97\ (3.61)$ kA/cm^2 and near threshold slope efficiency of 0.27 (0.36) W/A, respectively. The internal loss, α_i, and internal quantum efficiency, η_i, extracted from the cavity length dependent characteristics, are $13 \pm 0.5\ (11 \pm 0.5)$ cm^{-1} and $\sim$65 ($\sim$80) %, respectively. The increase (decrease) in $\alpha_i\ (\eta_i,)$ values suggests enhanced loss mechanism in the QCW mode, partly attributed to the junction heating. Note that the $L-I$ curve of the QCW mode show abrupt kinks at $\sim 5.9J_{th}$, and $\sim 8.0J_{th}$ while a comparatively linear power curve is seen in the SPW mode. These kinks are the indication of intense photon re-absorption in the highly inhomogeneous system, which is happening at a particular injection levels, and switching lasing actions from different confined energy levels due to the onset of additional Fabry-Perot modes [14]. The formation of a reduced intensity gap within the lasing spectra around these pumping levels further confirm enhanced photon loss in the system. The spectra appears to be comprised of three groups of longitudinal modes; the short wavelength (SM), long wavelength (LW), with a quenched middle wavelength (MW) group in between. This dictates that three dash groups governs the lasing operation, similar to our observation in the SPW modes [Fig. 3(c)] [15]. To further support our postulation, we studied the cavity length dependent gain characteristics under the QCW mode. Fig. 4(a) shows the

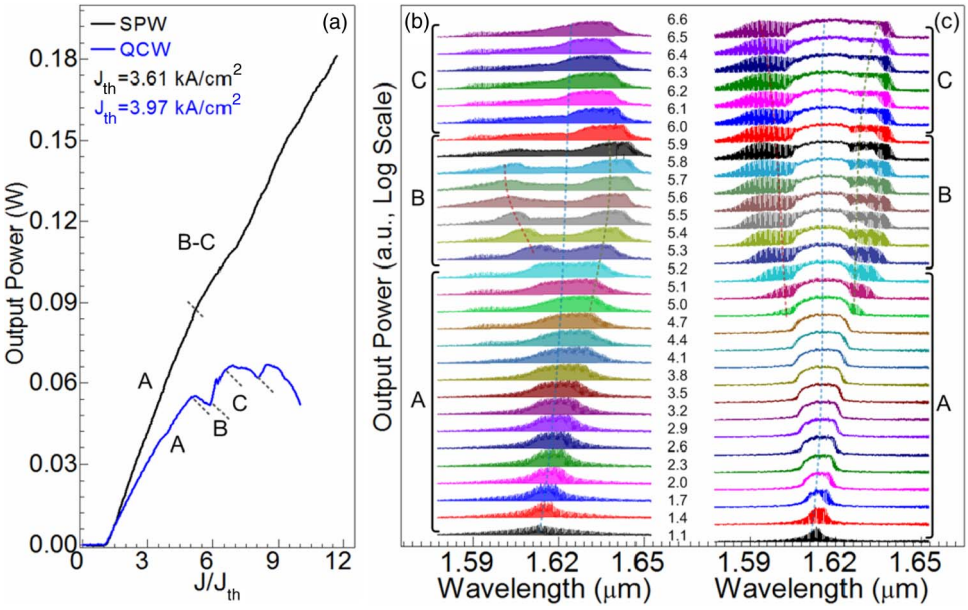

Fig. 3. (a) $L-I$ characteristics of 2×830 μm^2 laser at QCW and SPW operations. The broken lines roughly indicate the kinks and the injection range of Regions *A*, *B*, and *C*. Progressive lasing spectra (Log scale) at different current injection for (b) QCW and (c) SPW operations. The square brackets in (b) and (c) show the various pumping regions, and the numbers on the vertical scale in between (b) and (c) correspond to the current injection value ($\times J_{th}$). The red, blue, and green dashed lines are the guide to the eyes indicating the *Q*20, *Q*15, and *Q*10 dash groups, respectively. Note that Region *C* is at the verge of optical power roll-off.

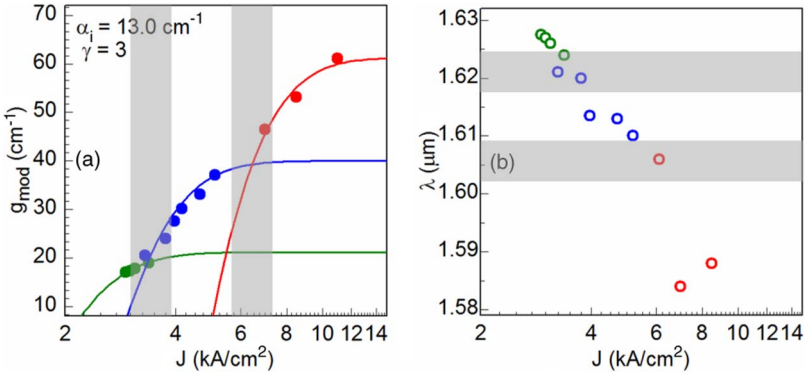

Fig. 4. (a) Modal gain of CQD laser structure and (b) $1.1J_{th}$ lasing wavelength, versus threshold current density at room temperature, obtained from devices with different cavity lengths (250–3000 μm), at QCW operation. The solid lines in (a) are the theoretically fitted curves using Eqn. (1) with non-ideality factor $\gamma = 3$ and internal loss $\alpha_i = 13$ cm^{-1}. The shaded regions vaguely separate the dominant three Qdash groups corresponding to the *Q*10, *Q*15, and *Q*20 stacking layers.

experimental dependence of the modal gain on the injection current density, obtained at various cavity lengths. Fitting the data points by the well known empirical gain expression [2], [3], [16]:

$$g_{\mathrm{mod}} = g_{sat}\left[1 - \exp\left(-\frac{(J - J_0)}{J_0}\right)\right] \tag{1}$$

revealed three gain curves instead of one, with extracted transparency current density J_0 (saturated modal gain, g_{sat}) of 1.9 kA/cm^2 (21 cm^{-1}), 2.7 kA/cm^2 (40 cm^{-1}), and 4.8 kA/cm^2 (60 cm^{-1}); representative of emission from *Q*10, *Q*15, and *Q*20 dash groups [see Fig. 1(a)], respectively. We

note that J_0 (g_{sat}) attains large values in the QCW mode compared to the SPW mode [15] owing to the larger value of internal loss (due to increased absorption process) which requires more number of carriers to compensate for the loss and reach population inversion, in general. Fig. 4(b) shows the near threshold lasing wavelength of various cavities tested, from which the qualitative emission boundaries of the three Qdash groups are identified (shaded gray region) approximately at 1608 nm ($\pm$6 nm) and 1622 nm ($\pm$6 nm). In what follows, we addressed qualitatively the cause of this anomalous spectral behavior from the view point of the highly dispersive dot-like and wire-like nature of dashes, i.e. the inhomogeneous broadening of the active region. For simplicity, we divide the lasing spectra into three regions *A*, *B*, and *C* (low, moderate and high injections, respectively) and explain the lasing operation in each region individually.

Region *A* in Fig. 3(b) shows a typical lasing operation where the lasing is initiated at $\sim$1614 nm (onset of lasing from the *Q*15 dashes) and the spectra subsequently broadens with increasing injection as more dashes within the ensemble and from adjacent stacks $(Q20)$ starts lasing concurrently. In addition, lasing from higher sub-bands of these dashes, due to band filling effect, might also broaden the spectra, which is possible in a highly inhomogeneous system owing to the availability of their highly dispersive ground state energy levels and overlapping high energy tail states. A smooth $L-I$ curve in this regime $(\sim\leq 5.0J_{th})$ indicates a normal laser diode operation, showing no signs of any optical power loss.

Distinct lasing behavior is observed in Region *B* where a broad single lasing lobe splits into SW (*Q*20 dashes) and LW (*Q*10 dashes) longitudinal modes group, separated by a low intensity MW (*Q*15 dashes) group. The quenching of *Q*15 dashes that behaves as carrier feeder to *Q*10 dashes further reduces in quantum efficiency on current pumping and the gap widens along with the blue (red) shift of SW (LW) group of longitudinal modes. This observation is attributable to the increase in the carrier feeding mechanism as a result of more dashes attaining population inversion from *Q*10 dash group. The shifting of the SW(LW) groups is a result of simultaneous lasing by different dashes from the respective *Q*20 $(Q10)$ stacks. Moreover, the observation of sharp kink with drastic decrease in the slope of $L-I$ curve around $\sim 5.2J_{th}$ to $5.9J_{th}$ is a signature of intense photon re-absorption process occurring in the system, due to the photon-carrier coupling between different dash groups as determined by the active region inhomogeneity.

In the high injection region (Region *C*), broadening and blue shifting of LW modes, and quenching of SW lasing modes is observed, as shown in Fig. 3(b). This indicates a gradual shift in the absorption process from *Q*15 to *Q*20 dash groups thereby progressively increasing the quantum efficiency of *Q*15 dashes. In other words, the single lobe spectra in this region is a collective lasing from *Q*15, in part, and *Q*10 dashes rather than only *Q*10 dashes. A sharp increase in the slope of $L-I$ curve in this regime ($\sim 6.0J_{th}$ to $6.6J_{th}$) further support our attribution of simultaneous lasing from these two dash ensembles.

A similar atypical lasing operation in observed in all the tested laser diodes in the QCW mode. For instance, we show the lasing characteristics of a long cavity 2×1600 μm^2 CQD laser at room temperature in Fig. 5. Note that a comparable lasing behavior is observed in Regions *A* and *B*, while Region *C* is more clearly visible in this case since the device heating is minimum compared to the short cavity laser wherein Region *C* was at the verge of optical power roll-off. The formation of a single lobe broad emission spectrum (FWHM $\sim$ 23 nm at $3.8J_{th}$), in Region *C*, because of collective lasing from *Q*15 to *Q*10 dashes, is apparent from Fig. 5(b). Moreover, further increase in current pumping leads to yet another splitting of the emission spectra, suggesting a periodic behavior. This is possible in a carrier deficient system (*i.e.*, the QCW mode) where the possibility of thermal carrier spillover is high leading to non-uniform thermal re-distribution of carriers among Qdash stacks that would affect the active region gain, and hence the lasing spectra. Note that the spectral position of the low intensity gap depends on the drive current and therefore we rule out the possibility of any lateral cavity resonances [17] or leaky substrate modes [18] in our device that might cause such anomalous observation. However, we cannot exclude the possibility of different non-linear phenomena occurring in the active region that affects the lasing spectra, particularly, the spectral and spatial hole burning effects which intensifies with continuous surge of carriers and/or temperature rise.

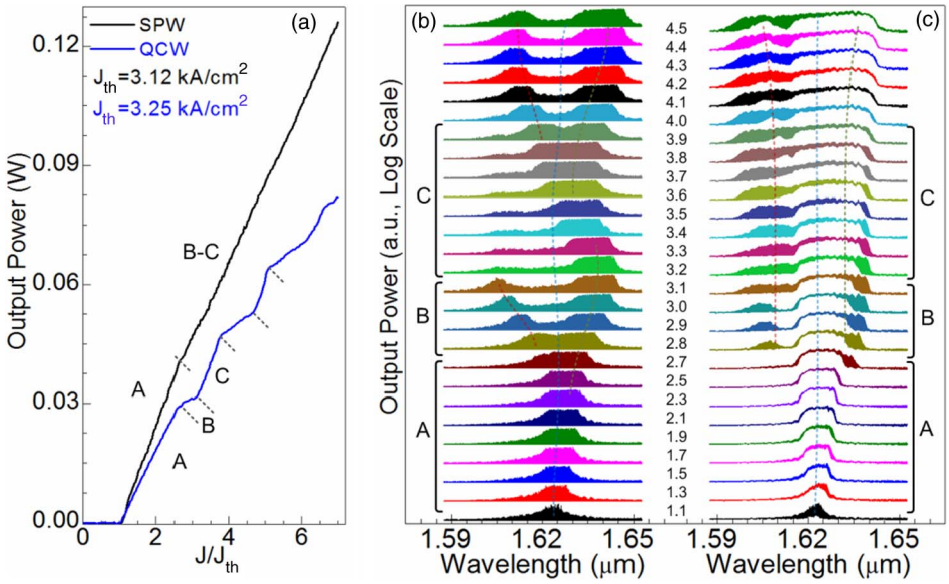

Fig. 5. (a) $L-I$ characteristics of 2×1600 μm^2 laser at QCW and SPW operations. The broken lines roughly indicate the kinks and the injection range of Regions *A*, *B*, and *C*. Progressive lasing spectra (Log scale) at different current injection for the (b) QCW and (c) SPW operations. The square brackets in (b) and (c) show the various pumping regions, and the numbers on the vertical scale in between (b) and (c) correspond to the current injection value ($\times J_{th}$). The red, blue, and green dashed lines are the guide to the eyes indicating the *Q*20, *Q*15, and *Q*10 dash groups, respectively.

In the following, we attempt to explain the carrier feeding (via optical pumping) mechanism, which dominates the lasing behavior in the QCW mode, qualitatively by referring to the energy band model shown in Fig. 1(a). Consider laser emission originating from the *Q*15 dashes once the total device loss is compensated. Since these dispersive nanostructure posses highly overlapping quasi zero-dimensional DOS, generally, onset of lasing occurs via average intermediate height ($Q15$) dash group [19]–[21]. By increasing the continuous surge of carriers (which is the case of QCW mode), a majority of the generated photons from *Q*15 dashes starts to get absorbed in *Q*10 dashes (due to their large average height and DOS, and small band transition energies). Since *Q*20 dashes energy levels appears at the tail of *Q*10 dashes DOS, negligible photon absorption from these dashes takes place. When *Q*10 dashes start reaching population inversion, the rate of photon re-absorption from *Q*15 increases drastically. This quenches the intensity of *Q*15 dashes considerably, and their rate of acquiring photon from lasing *Q*20 dashes (due to their smaller average height, lower DOS, and hence less photon generation) is comparatively low. Meanwhile, at high injections, *Q*20 dashes is able to achieve population inversion and lase, apart from feeding *Q*15 dashes, because of their dot-like features and lower modal gain compared to the *Q*10 and *Q*15 dashes. This non-uniform distribution of carriers in the highly inhomogeneous active region creates a reduced intensity gap due to *Q*15 (MW modes) dash group operating between the *Q*20 (SW modes) and *Q*10 (LW modes) dashes. Note that the QCW mode is further influenced by junction heating, demonstrated by reduced internal quantum efficiency in this case. Therefore the carrier spill-over (thermally activated carrier leakage) mechanism is comparatively high in small band offsets dash ensembles (*i.e.*, *Q*20 and *Q*15) which further reduces their efficiency, particularly *Q*15 dashes, compared to *Q*10 dash groups. Moreover, the availability of absorption (mainly from Q15 dash stack) and gain (from *Q*10 and *Q*20 dash stacks) portions within the active medium might lead to device self pulsation, an attractive design feature in the field of passive mode locking.

Comparing Figs. 3(b) and 5(b) reveal another observation; an earlier occurrence of Region *B* (at $\sim 2.8 J_{th}$) or the spectra splitting in the 1600 μm laser compared to the 830 μm laser (at $\sim 5.2 J_{th}$). We attribute this to the earlier start of carrier feeding mechanism from the *Q*15 dash groups in the former case compared to the latter case. The onset of lasing from the long cavity laser is from the

lower transition energy end of the $Q15$ group ($\sim$1620 nm), implying that the photon re-absorption process by the $Q10$ dash group has already started (from the higher transition energy $Q15$ dashes). Therefore, feeding and lasing simultaneously probably results in an early gain saturation of $Q15$ dashes and reduction of their emission intensity on subsequent injection, owing to more $Q10$ dashes attaining population inversion. In the case of short cavity device, the lasing is initiated from the central transition energy of $Q15$ group ($\sim$1613 nm) which leaves more number of low transition energy $Q15$ dashes to feed the $Q10$ dash group, even at very high injection. Therefore, the probability of $Q15$ group attaining gain saturation, in this case, is at comparatively large pumping values.

The lasing operation under the SPW mode is observed to be similar in both the laser diodes, depicting dominance from three Qdash groups [15]. Referring to Figs. 3(c) and 5(c), the progressive broadening of the lasing spectra with increasing current injection, is apparent in Region *A*, and very similar to that of QCW operation. The onset of lasing initiates from the $Q15$ dash group (MW modes), and a smooth $L - I$ curve is observed. Region *B* depicts onset of lasing from the $Q20$ (SW modes) and $Q10$ (LW modes) dash groups and the current value agrees well with that of the QCW mode wherein the spectral split is observed. This further supports our attribution of three dash groups governing the lasing behavior in both the current operations. Subsequent current pumping appreciably overlaps the ground state emissions of the $Q15$ and $Q10$ dash ensembles, suggesting uniform distribution of dash states among these highly inhomogeneous stacks. The visible Fabry-Perot resonance in the SW modes suggests photon re-absorption occurring in the active medium that prevents this dash group to compete evenly with other dash groups. However, a weak kink and a slight decrease in the slope of $L - I$ curve in this region indicates that this process is insignificant. Thereafter, subsequent injection contributed to the progressive broadening of lasing spectra with a single emission lobe, which indicates that SPW as a carrier sufficient system. This broadening is a result of simultaneous lasing from all the three dash groups evenly, and with a smooth $L - I$ curve. The measured bandwidth (at FWHM) from the short and long cavity lasers under SPW (QCW) operations are $\sim$27 ($\sim$37) nm at $\sim 6J_{th}(\sim 4.5J_{th})$, and $\sim$50 ($\sim$40) nm at $\sim 11J_{th}$ $(\sim 5.5J_{th})$, respectively. These values are larger by $\sim$50% (20%) from our previously reported as-grown (intermixed) fixed barrier Qdash laser structure [1]–[3]. This shows that the chirped barrier thickness structure along with Qdash nano-structures are promising candidates in realizing broadband emission devices.

4. Conclusion

In conclusion, we studied the room temperature stimulated emission characteristics of the chirped Qdash ridge-waveguide laser diode operating in the L–communication band, at two different pulsed durations. The peculiar spectral characteristics of spectral split under the QCW mode, from this class of active material, have been addressed qualitatively based on the carrier-photon re-distribution among the Qdash DOS, together with the highly inhomogeneous active region. A broad stimulated emission spectrum (FWHM) as large as 50 nm, under the SPW operation demonstrates the feasibility of chirped epitaxial design in realizing broad gain/broad emission devices, particularly in high power broadband laser diode platform.

References

[1] C. L. Tan, H. S. Djie, Y. Wang, C. E. Dimas, V. Hongpinyo, Y. H. Ding, and B. S. Ooi, "Wavelength tuning and emission width widening of ultrabroad quantum dash interband laser," *Appl. Phys. Lett.*, vol. 93, no. 11, pp. 111101-1–111101-3, Sep. 2008.

[2] B. S. Ooi, H. S. Djie, Y. Wang, C. L. Tan, J. C. M. Hwang, X. M. Fang, J. M. Fastenau, A. W. K. Liu, G. T. Dang, and W. H. Chang, "Quantum dashes on InP substrate for broadband emitter applications," *IEEE J. Sel. Topics Quantum Electron.*, vol. 14, no. 4, pp. 1230–1238, Jul./Aug. 2008.

[3] H. S. Djie, C. L. Tan, B. S. Ooi, J. C. M. Hwang, X. M. Fang, Y. Wu, J. M. Fastenau, W. K. Liu, G. T. Dang, and W. H. Chang, "Ultrabroad stimulated emission from quantum-dash laser," *Appl. Phys. Lett.*, vol. 91, no. 11, pp. 111116-1–111116-31, Sep. 2007.

[4] M. Z. M. Khan, T. K. Ng, C.-S. Lee, P. Bhattacharya, and B. S. Ooi, "Effect of optical waveguiding mechanism on the lasing action of chirped InAs/AlGaInAs/InP quantum dash lasers," in *Proc. SPIE*, 2013, pp. 864005-1–864005-6.
[5] A. Kovsh, I. Krestnikov, D. Livshits, S. Mikhrin, J. Weimert, and A. Zhukov, "Quantum dot laser with 75 nm broad spectrum of emission," *Opt. Lett.* , vol. 32, no. 7, pp. 793–795, Apr. 2007.
[6] C.-S. Lee, W. Guo, D. Basu, and P. Bhattacharya, "High performance tunnel injection quantum dot comb laser," *Appl. Phys. Lett.*, vol. 96, no. 10, pp. 101107-1–101107-3, Mar. 2010.
[7] F. Lelarge, B. Dagens, J. Renaudier, R. Brenot, A. Accard, F. van Dijk, D. Make, O. Le Gouezigou, J. G. Provost, and F. Poingt, "Recent advances on InAs/InP quantum dash based semiconductor lasers and optical amplifiers operating at 1.55 m," *IEEE J. Sel. Topics Quantum Electron.*, vol. 13, no. 1, pp. 111–124, Jan./Feb. 2007.
[8] J. P. Reithmaier, G. Eisenstein, and A. Forchel, "InAs/InP quantum-dash lasers and amplifiers," *IEEE Proc.*, vol. 95, no. 9, pp. 1779–1790, Sep. 2007.
[9] H. S. Djie, C. E. Dimas, and B. S. Ooi, "Wideband quantum-dash-in-well superluminescent diode at 1.6 mm," *IEEE Photon. Technol. Lett.*, vol. 18, no. 16, pp. 1747–1749, Aug. 2006.
[10] Z. Y. Zhang, R. A. Hogg, X. Q. Lv, and Z. G. Wang, "Self-assembled quantum-dot superluminescent light-emitting diodes," *Adv. Opt. Photon.*, vol. 2, no. 2, pp. 201–228, Jun. 2010.
[11] F. Grillot, N. A. Naderi, M. Pochet, C. Y. Lin, and L. F. Lester, "Variation of the feedback sensitivity in a 1.55 μm InAs/InP quantum-dash Fabry–Perot semiconductor laser," *Appl. Phys. Lett.*, vol. 93, no. 19, pp. 191108-1–191108-3, Nov. 2008.
[12] A. Somers, W. Kaiser, J. P. Reithmaier, A. Forchel, M. Gioaninni, and I. Montrosset, "Optical gain properties of InAs/InAlGaAs/InP quantum dash structures with a spectral gain bandwidth of more than 300 nm," *Appl. Phys. Lett.*, vol. 89, no. 6, pp. 061107-1–061107-3, Aug. 2006.
[13] C. L. Tan, H. S. Djie, and B. S. Ooi, "Novel multiwavelength emitter for WDM transmission utilizing broadband quantum-dash laser diode," in *Proc. CLEO*, 2009, pp. 1–2.
[14] C. L. Tan, H. S. Djie, Y. Wang, C. E. Dimas, V. Hongpinyo, Y. H. Ding, and B. S. Ooi, "The influence of nonequilibrium distribution on room-temperature lasing spectra in quantum-dash lasers," *IEEE Photon. Technol. Lett.*, vol. 21, no. 1, pp. 30–32, Jan. 2009.
[15] M. Z. M. Khan, T. K. Ng, C.-S. Lee, P. Bhattacharya, and B. S. Ooi, "Chirped InAs/InP quantum-dash laser with enhanced broad spectrum of stimulated emission," *Appl. Phys. Lett.*, vol. 102, no. 9, pp. 091102-1–091102-3, Mar. 2013.
[16] A. Zhukov, A. Kovsh, V. Ustinov, A. Y. Egorov, N. Ledentsov, A. Tsatsul'Nikov, M. Maximov, Y. M. Shernyakov, V. Kopchatov, and A. Lunev, "Gain characteristics of quantum dot injection lasers," *Semicond. Sci. Technol.*, vol. 14, no. 1, p. 118, Jan. 1999.
[17] D. Ouyang, R. Heitz, N. N. Ledentsov, S. Bognar, R. L. Sellin, C. Ribbat, and D. Bimberg, "Lateral-cavity spectral hole burning in quantum-dot lasers," *Appl. Phys. Lett.*, vol. 81, no. 9, pp. 1546–1548, Aug. 2002.
[18] A. Patane, A. Polimeni, L. Eaves, M. Henini, P. C. Main, P. M. Smowton, E. J. Johnston, P. J. Hulyer, E. Herrmann, and G. M. Lewis, "Experimental studies of the multimode spectral emission in quantum dot lasers," *J. Appl. Phys.*, vol. 87, no. 4, pp. 1943–1946, Feb. 2000.
[19] M. Z. M. Khan, T. K. Ng, U. Schwingenschlogl, P. Bhattacharya, and B. S. Ooi, "Modeling the lasing spectra of InAs/InP quantum dash lasers," *Appl. Phys. Lett.*, vol. 98, no. 10, pp. 101105-1–101105-3, Mar. 2011.
[20] M. Z. M. Khan, T. K. Ng, U. Schwingenschlogl, P. Bhattacharya, and B. S. Ooi, "Effect of the number of stacking layers on the characteristics of quantum-dash lasers," *Opt. Exp.*, vol. 19, no. 14, pp. 13 378–13 385, Jul. 2011.
[21] M. Z. M. Khan, T. K. Ng, U. Schwingenschlogl, and B. S. Ooi, "Spectral analysis of quantum dash lasers: Effect of inhomogeneous broadening of the active gain region," *IEEE J. Quantum Electron.*, vol. 48, no. 5, pp. 608–615, May 2012.